

Numerical Simulation of Micro-Pattern Gaseous Detectors

A project report submitted by

Danush S

Supervised by

**Prof. Supratik Mukhopadhyay,
Saha Institute of Nuclear Physics**



July - September, 2020

Acknowledgments

I would start by thanking Prof. Supratik Mukhopadhyay for providing me the opportunity to work under his guidance for this project, which has been a tremendous factor into shaping my further interests in research. He has been patient, open and supportive to new ideas throughout the project. I would also like to thank Vishal Kumar for also guiding me throughout this project, from whom I also learnt some simple tricks to make code faster. I thank Prof. Bedangadas Mohanty and Dr. Varchaswi K. S. Kashyap for allowing me to access NISER's computers for using COMSOL Multiphysics, without their permission this part of the project would have been disrupted. I would also thank Dr. Abhik Jash, Soumik Chandra, and Aman Upadhyay their help and motivation they have provided me. Finally, and definitely equally important as the above acknowledgments, I thank my parents, family and friends for their support.

Abstract

This project involves studying and running simulations of the neBEM solver in Garfield++. Initially papers related to the important concepts behind neBEM was read and then simulations using the same were done on the Thick-Gaseous Electron Multiplying detector. We compared our results with an industry standard FEM solver, COMSOL Multiphysics®. Then, our focus shifted to simulating different meshes of the Micromegas and Bulk Micromegas detectors. The electric fields, gain and drift lines of the same were also studied. Simulations of the same configurations was also carried out on COMSOL Multiphysics® to compare it with the electric field values obtained using neBEM.

Contents

1	Introduction	4
1.1	Energy loss of particles passing through matter	5
1.2	Interaction of charged and neutral particles	5
1.3	Interaction of photons	5
1.4	Brief account of gaseous detectors	6
1.4.1	The Thick-GEM detector	7
1.4.2	The micromegas detector	8
2	The nearly exact Boundary Element Method	9
3	Simulation Work	12
3.1	Electric field calculations for a Thick-GEM detector	12
3.1.1	Qualitative comparison of neBEM and COMSOL results	13
3.1.2	Effects of Parametrization	15
3.2	Electric field calculations for the MicroMegas detector	16
3.2.1	The MicroMegas detector (with a calendared mesh)	17
3.2.2	The Bulk MicroMegas detector	21
4	Conclusions	27

Chapter 1

Introduction

There are multiple ways to simulate microscopic processes of a detector (especially gaseous detectors) used in High Energy Physics experiments. Depending on the requirements of an experiment, there is also a need to study or simulate the electrostatic fields of a detector beforehand to provide us with information as to what configuration to use in the experiment. Once information regarding the electric field is obtained, one can proceed to simulate the processes that occur in a detector to obtain information like gain, signal, resolution, etc. There are again different ways to simulate these microscopic processes, and further details on the same will be discussed in subsequent sections.

We can broadly classify this project into two parts: obtaining electric field information and plotting drift lines (and calculating other values like signal and gain) for two detectors, namely the Thick-Gas Electron Multiplier (Thick-GEM) and the Micromegas detector. The objective to perform these studies was to provide enough information to design the detector that would be made at Saha Institute of Nuclear Physics. Further details on the specifics will be discussed as we progress through the report.

A crucial objective in most nuclear or particle physics experiments is the detection of the radiation/particles that are emitted. It is thus important to look at how different particles and radiation interact with matter. This is one of the basis upon which detector designs are done. The variety of these processes is quite extensive and as a consequence, a large number of detection devices for particles and radiation exist. Depending on the energy of the incident radiation/particle, there are various methods for detection. A lot of advances have been made towards these detectors, and we will briefly go through some relevant detectors in this chapter, studying their structural design and the physics behind them. This chapter would mainly involve the description of the nearly exact Boundary Element Method, which is a numerical method to solve different physical properties like electric field values of a system in consideration.

1.1 Energy loss of particles passing through matter

In the case of gaseous detectors, information regarding the energy lost by an incident particle while it traverses through the gas is important. The Bethe-Bloch equation describes the energy loss (through many interactions) that heavy-charged particles like alpha particles undergo while traversing through a medium. There are also corrections to use the equation for light-charged particles like protons and electrons. The equation is as follows:

$$-\frac{dE}{dx} = 2\pi N_a r_e^2 m_e c^2 \rho \frac{Z}{A} \frac{z^2}{\beta^2} \left[\ln \left(\frac{2m_e \gamma^2 v^2 W_{\max}}{I^2} \right) - 2\beta^2 - \delta - 2\frac{C}{Z} \right] \quad (1.1)$$

where r_e and m_e are the radius and mass of an electron respectively, N_a is the Avogadro's number, I is the mean excitation potential, Z , A and ρ are the atomic number, atomic weight and density of the medium respectively, z and v are the charge and velocity of the incident particle respectively, δ and C are the density and shell correction terms respectively and W_{\max} is the maximum energy transfer possible in a single collision (obtained from kinematics).

Ref. [1] succinctly goes through the ins and outs of the Bethe-Bloch equation, the situations where this equation fails and when can it be used.

1.2 Interaction of charged and neutral particles

Charged particles are usually involved in electromagnetic interactions with the gas particles. Upon interaction with a charged particle, gas particles can undergo radiation-less rearrangements, dissociate or get excited or ionized, with the emission of photons or the appearance of free ion-electron pairs. At very high particle energy, other mechanisms like Bremsstrahlung and Cherenkov radiation can occur. Electrons and photons created by the primary encounters can further interact with the gas molecules, causing further ionizations called secondary ionizations. Charged particles can also undergo mechanical elastic collisions, and the slowing down in gas is mainly due to multiple inelastic processes of excitation and ionization.

Neutrons are particles with no charge and hence are not involved in any electromagnetic interaction with charged particles. But they can interact with other nuclei through processes like radioactive capture and nuclear reactions with the emission of particles (like protons, alpha particles, etc.) take place. Neutrons also interact with matter through elastic and inelastic scattering.

1.3 Interaction of photons

The interaction of photons with matter happen majorly through the Photoelectric effect, the Compton Effect and the Pair-Production Effect. Depending on the properties like the incident energy of the photon, the cross sections of each of these processes vary.

The photoelectric effect refers to the emission of electrons when a photon interacts with it. It occurs when the energy of the incident photon is higher but around the magnitude of the ionization energy of the atom. Sometimes the photon can eject an inner shell electron followed by rearrangement of electrons in the atom producing another photon or electron during the process.

Compton effect occurs when the energy of the incident photon is to some extent greater than the ionization energy of the atom. It is the process of transferring some of the energy and momentum to an electron the photon collides with.

The Pair-Production effect is observed when the incident photon is of energy greater than twice the mass of an electron. Pair production often refers to a photon creating an electron-positron pair near a nucleus.

The above interactions should cover a majority of possible interactions, but things get complicated when the medium does not comprise of just single atoms, but a mixture of atoms and molecules. For example, in molecular gases, energy can also be spent in rotational, vibrational energy, etc. An account of more than 20 processes that can follow the inelastic interaction of electrons and molecules are provided in [meek].

1.4 Brief account of gaseous detectors

The working principle behind gaseous detectors involves detecting incoming particles by producing a readable electric current through ionization of the gas particles. The particles we wish to detect enters the gaseous detector, ionizes the atoms/molecules of the medium and produces one or more primary ion-electron pairs depending on factors like the energy of the incident particle. Due to the external electric field, usually, these electrons accelerate and gain enough energy to create secondary interactions and produce more ion-electron pairs. Under these conditions, the number of electrons grows rapidly forming an avalanche multiplication (also called as the Townsend Avalanche), thus producing a readable electric signal on the electrodes [thesis]. There are different innovative designs of gaseous detectors to achieve the above characteristics. One of the early ones was the Multi-Wire Proportional Chamber which consisted of a set of thin, parallel and equally spaced anode wires, symmetrically placed between two cathode planes. Another example is the Micro-Strip Gas Counter that had an upper drift electrode and thin parallel metal strips, alternating wide (anodes) and narrow (cathodes) laid on an insulating support usually at a pitch of a few hundred microns. Schematic diagrams of the same are as seen in Figures ?? and ?. Since our simulations involve the Thick-GEM and Micromegas detectors, the following subsections goes into brief description of detectors.



Figure 1.1: Schematic diagram of a (a) Multi-Wire Proportional Counter and a (b) Micro-Strip Gas Counter. Source: [2]

1.4.1 The Thick-GEM detector

The Thick-GEM detector is in some ways an improvement of the Gas Electron Multipliers (GEM) where the delicacy of the foil was undesirable. The Thick-GEM is a physically a more durable detector with the ability to sustain electrical discharges. It also gives a much higher gain, making it easy to read the currents. But GEMs offer better spatial resolution than compared to Thick-GEMs. The Thick-GEM foil is made of PCB board (the PCB material, usually FR4, is generally around 0.4-0.8mm thick, but thicker materials are used in research) with copper clads on both side. The board is perforated by holes of a cylindrical shape (usually with a diameter of 0.5mm), and these holes can be mechanically drilled, which makes it cheaper to make than compared to GEMs (which need etching techniques). High voltages are applied on both copper surfaces to provide for a high voltage gradient. The electric field across the Thick-GEM electrode is generally around 25kV/cm. The foil is placed in between a drift electrode and readout pads (anode), all in an air-tight environment with a specific gas or combination of gases. Electrons deposited by the incident ionizing radiation in the drift region, drift towards the Thick-GEM foil under the drift field and then are focused into the dipole field within the micron-hole. The shape of the hole ensures a high dipole field and a more focused electron path at the center. The readout pads under the foil to collect all charges that come through the foil. When an ionizing particle passes through, it produces primary charges by ionization above the electrode, and by means of drift and diffusion processes, the charges are transported through the gas volume to the amplification region close to the electrodes and these charges will attain high velocities due to the high electric field and cause further ionizations leading to an avalanche effect. Separated from the multiplying electrode, the charge collection and readout plane can be patterned at will with strips or pads; usually, they are a set of perpendicular strips to serve as a 2-dimensional projective readout.

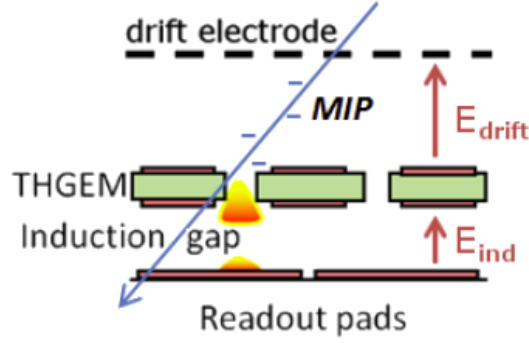


Figure 1.2: Schematic diagram of the Thick-GEM detector setup. Source: [3]

1.4.2 The micromegas detector

MICROMEGAS (for MICRO MESH Gaseous Structure) is just like the Thick-GEM, but instead of the Thick-GEM foil that was placed in between the drift electrode and the readout, we now have a very thin micromesh. The working principle is similar to that of the Thick-GEM. In a Micromegas detector, this gas volume is divided in two by a metallic micro-mesh placed, but the multiplication region is very narrow compared to the region above the mesh. This project tries to simulate a calendered mesh and a mesh where the wires are woven into other wires. The results of which are discussed in the subsequent sections.

Chapter 2

The nearly exact Boundary Element Method

As mentioned earlier, in order to simulate microscopic processes we first need the electric field values of the system in consideration. Analytic methods to provide for the same are very accurate although finding such solutions for systems with complex structures can be very difficult. This is where numerical methods like the Finite Element Method (FEM) and Boundary Element Method (BEM) come into the picture. FEM involves calculating potential at nodes, and the potential value at any other point is obtained using interpolation which can result in inaccuracies. One can increase the number of nodes to reduce the error from inaccuracies but this would need high computational resources or time[4]. FEM also cannot provide enough number of nodes near a tip or sharp surface.

BEM which is a numerical implementation of Boundary Integral Method, where the electrode surfaces are divided into regions each of which is assumed to carry a uniform free charge density. The potential at an arbitrary point is calculated by summing the contributions from the charge density (which is calculated by satisfying the Dirichlet/Neumann type boundary conditions for the given device through a suitable Green's function formulation) on each region. But this method cannot produce acceptable results close to geometric singularities (like corners or edge) [5].

Recently, a new approach using analytic expressions for fields, but in the formulation of BEM was proposed, which leads to their nominally exact evaluation [4]. The nearly exact Boundary Element Method (neBEM) solver uses a closed form expressions of the potential and the field obtained from the symbolic integration of the Green's function of a uniform charge density distributed over flat triangular or rectangular boundary element. neBEM first breaks up the system of interest into right triangles and rectangles (they are referred to as primitives) and then the contribution from a primitive (assuming charge is uniformly distributed) is calculated using a closed form expressions (analytical solutions) of the potential and the field obtained from the symbolic integration of the Green's function [6]. Unlike BEM, this method is capable of yielding accurate values even in the near-field region.

In the present approach, namely NEBEM, the influences are calculated using analytic solution of potential and electrostatic field due to a uniform charge distribution over a flat rectangular surface. The equations of the same are in [4]. It may be noted here that, in neBEM, any three-dimensional device is assumed to be composed of a number of flat surfaces called primitives. These surfaces can be right-triangular or rectangular. Thus, in the pre-processing stage, the device of interest needs to be segmented into right triangles or rectangles (See [6]).

If given a uniformly charged rectangle (on the XZ plane) with the two diagonally opposite corners at $(x_1, 0, z_1)$ and $(x_2, 0, z_2)$, [4] has obtained the closed form expression of the potential at an arbitrary point (X, Y, Z) , given by:

$$\begin{aligned} \phi(X, Y, Z) = & (X - x_1) \ln \left(\frac{D_{12} - (Z - z_2)}{D_{11} - (Z - z_1)} \right) + (X - x_2) \ln \left(\frac{D_{21} - (Z - z_1)}{D_{22} - (Z - z_2)} \right) \\ & + (Z - z_1) \ln \left(\frac{D_{21} - (X - x_2)}{D_{11} - (X - x_1)} \right) + (Z - z_2) \ln \left(\frac{D_{12} - (X - x_1)}{D_{22} - (X - x_2)} \right) \\ & + \frac{i|Y|}{2} \times \left(S_1 \left(\tanh^{-1} \left(\frac{R_1 + iI_1}{D_{11}|Z - z_1|} \right) - \tanh^{-1} \left(\frac{R_1 - iI_1}{D_{11}|Z - z_1|} \right) \right. \right. \\ & + \tanh^{-1} \left(\frac{R_1 - iI_2}{D_{21}|Z - z_1|} \right) - \tanh^{-1} \left(\frac{R_1 + iI_2}{D_{21}|Z - z_1|} \right) \Bigg) \\ & + S_2 \left(\tanh^{-1} \left(\frac{R_2 + iI_2}{D_{22}|Z - z_2|} \right) - \tanh^{-1} \left(\frac{R_2 - iI_2}{D_{22}|Z - z_2|} \right) \right. \\ & \left. \left. + \tanh^{-1} \left(\frac{R_2 + iI_1}{D_{12}|Z - z_2|} \right) - \tanh^{-1} \left(\frac{R_2 - iI_1}{D_{12}|Z - z_2|} \right) \right) \right) - 2\pi Y \end{aligned} \quad (2.1)$$

where $D_{ij} = \sqrt{(X - x_i)^2 + Y^2 + (Z - z_j)^2}$, $R_i = Y^2 + (Z - z_i)^2$, $I_i = (X - x_i)|Y|$ and $S_i = \text{sign}(z_i - Z)$.

If given a uniformly charged right triangle element (on the XZ plane) with three vertices on $(0, 0, 0)$, $(1, 0, 0)$ and $(0, 0, z_M)$, [5] has obtained the closed form expression of the potential at an arbitrary point (X, Y, Z) , given by:

$$\begin{aligned} \Phi = & \frac{1}{2} ((z_M Y^2 - XG)(LP_1 + LM_1 - LP_2 - LM_2) + i|Y|(z_M X + G)(LP_1 - LM_1 - LP_2 + LM_2) \\ & - S_1 X \left(\tanh^{-1} \left(\frac{R_1 + iI_1}{D_{11}|Z|} \right) + \tanh^{-1} \left(\frac{R_1 - iI_1}{D_{11}|Z|} \right) \right. \\ & \left. - \tanh^{-1} \left(\frac{R_1 + iI_2}{D_{21}|Z|} \right) - \tanh^{-1} \left(\frac{R_1 - iI_2}{D_{21}|Z|} \right) \right) \end{aligned} \quad (2.2)$$

where D_{ij} , R_i , S_i are the same as ones used in Equation 2.1, $E_1 = (X + z_M^2 - z_M Z)$, $E_2 = (X - 1 - z_M Z)$, $G = z_M(X - 1) + Z$, $H_1 = Y^2 + G(Z - z_M)$, $H_2 = Y^2 + GZ$, $LP_1 = \frac{1}{G - iz_M|Y|} \log \left(\frac{(H_1 + GD_{12}) + i|Y|(E_1 - z_M D_{12})}{-X + i|Y|} \right)$, $LM_1 = \frac{1}{G + iz_M|Y|} \log \left(\frac{(H_1 + GD_{12}) - i|Y|(E_1 - z_M D_{12})}{-X - i|Y|} \right)$,

$$LP_2 = \frac{1}{G - iz_M|Y|} \log \left(\frac{(H_2 + GD_{21}) + i|Y|(E_2 - z_M D_{21})}{1 - X + i|Y|} \right) \text{ and } LM_2 = \frac{1}{G + iz_M|Y|} \log \left(\frac{(H_2 + GD_{21}) - i|Y|(E_2 - z_M D_{21})}{1 - X - i|Y|} \right).$$

One important feature of neBEM, as explained in [5] is that the results obtained for electrostatic problems containing edges and singularities were numerically stable and physically acceptable, thus showcasing the accuracy, flexibility and robustness of using neBEM.

Chapter 3

Simulation Work

We attempted in simulating the Micromegas, Bulk Micromegas and Thick-GEM using different geometries in Garfield++ using the neBEM solver. For some results, the same simulations were done using COMSOL Multiphysics (which is a FEM solver) to compare plots obtained using neBEM.

The main interest of these simulations were with respect to the MicroMegas detector with the calendared meshes. The objective of simulating the MicroMegas detector (and multiple calendared meshes) was to purchase one of these meshes to use in an experiment to be conducted at Saha Institute of Nuclear Physics, Kolkata.

3.1 Electric field calculations for a Thick-GEM detector

All plots shown in this section are for a Thick-GEM detector with the following specifications:

1. ThickGEM foil made of Kapton and Copper.
2. Inner and outer hole diameter = 0.3mm and 0.4mm respectively.
3. Thickness of Kapton and Copper in Thick-GEM foil = 0.4mm and $5\mu\text{m}$ respectively.
4. Thickness of drift electrode and anode = $5\mu\text{m}$.
5. Pitch = 1mm.
6. Induction and drift gap = 1mm.
7. Voltages given to the drift electrode, upper Thick-GEM layer, bottom Thick-GEM layer and anode = -750V, -250V, 250V, and 750V respectively.
8. A Thick-GEM with a total of 50 holes was simulated.

3.1.1 Qualitative comparison of neBEM and COMSOL results

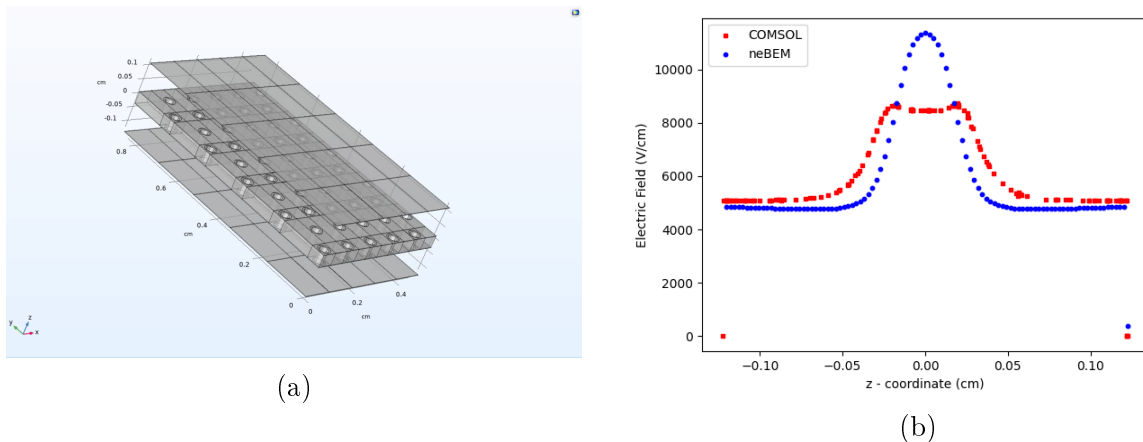


Figure 3.1: (a) The Thick-GEM detector as built in COMSOL and (b) a plot of the electric field across a line passing through the center of a hole obtained using neBEM and COMSOL.

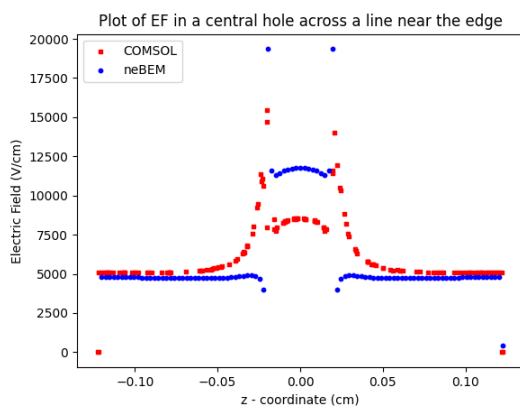
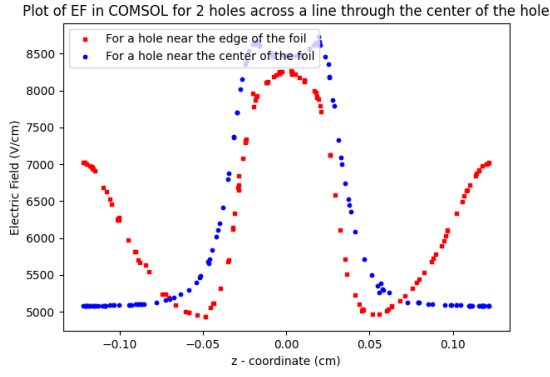
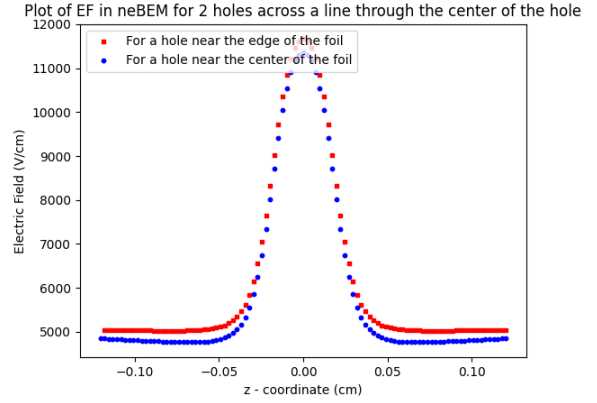


Figure 3.2: Plots of the electric field across a line passing through a hole at the center of the foil close to the hole wall. It compares neBEM and COMSOL.

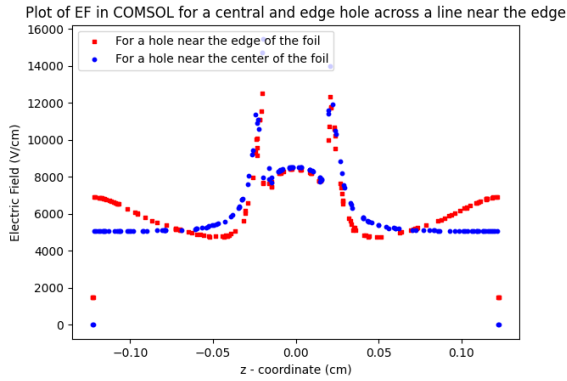


(a)

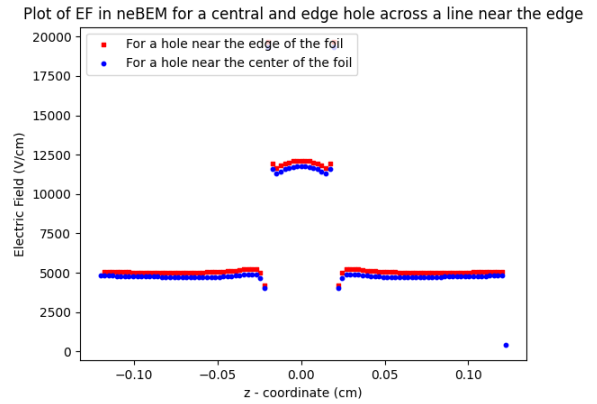


(b)

Figure 3.3: Plots of the electric field across lines passing near the hole wall, for 2 holes, one at the center of the foil and the other near the edge of the foil to look at edge effects. Plots (a) and (b) were done in COMSOL and neBEM respectively.



(a)



(b)

Figure 3.4: Plots of the electric field across lines passing through the center of the hole, for 2 holes, one at the center of the foil and the other near the edge of the foil to look at edge effects. Plots (a) and (b) were done in COMSOL and neBEM respectively.

From the above figures we see that there is an observed difference between results obtained using neBEM and COMSOL in magnitude and trends. From Figures 3.3a, 3.3b, 3.4a and 3.4b we observe some kind of effects induced at the edge, and also the differences between neBEM and COMSOL results at different regions of the detector foil.

3.1.2 Effects of Parametrization

There are a variety of parameters that we can control while running simulations in COMSOL and neBEM. The parameters we studied for neBEM are target element sizes (which give rise to different discretizations), number of panels, number of Thick-GEM holes, Periodic Boundary Conditions (PBCs), etc. We vary the number of Thick-GEM holes to reach a good position in the computation-accuracy trade-off as we would like to know how many holes we need to simulate, beyond which the values of the electric field saturate.

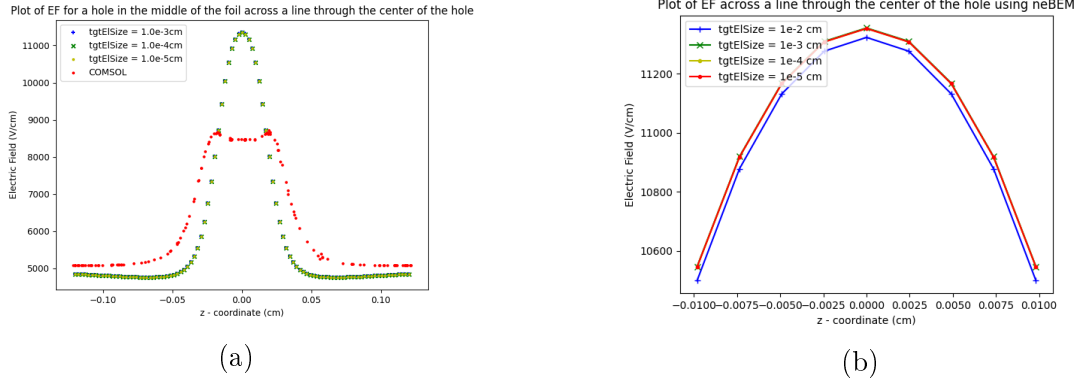


Figure 3.5: Plots of the electric field obtained using neBEM for different target element sizes across a line (a) through the entire height of the detector volume and (b) near the foil-region.

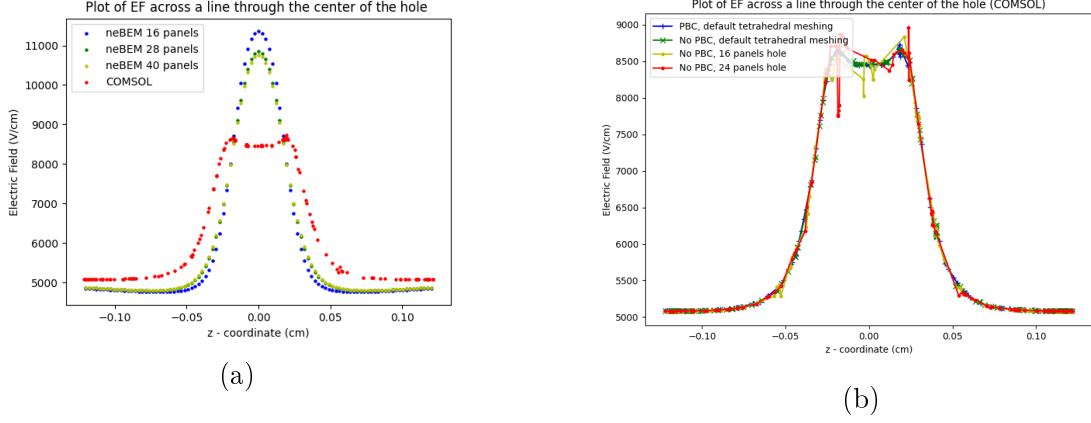


Figure 3.6: Plots of the electric field obtained (a) using neBEM for different panels (with a comparison of COMSOL) and (b) using COMSOL for different conditions like panel numbers, tetrahedral meshing and PBC.

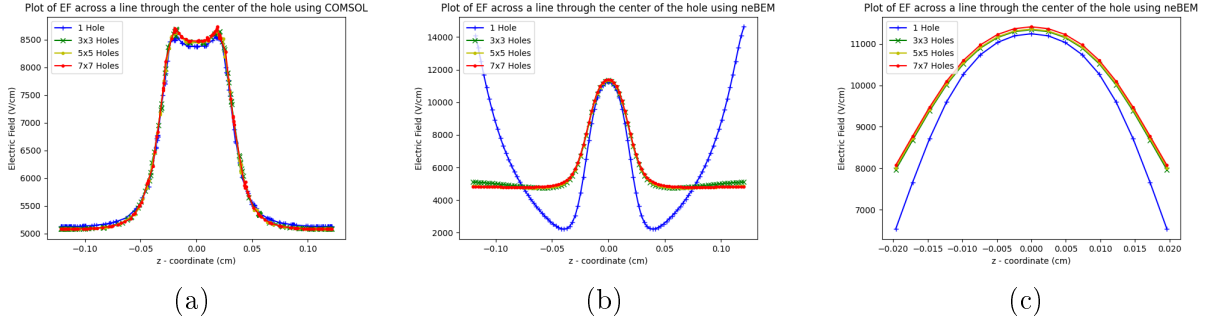


Figure 3.7: Plots of the electric field obtained for different Thick-GEM hole numbers (a) using COMSOL. (b) using neBEM and (c) using neBEM for different target element sizes (a) through the entire height of the detector volume and (b) across a line (c) across a line near the foil-region.

One inference we can make from Figure 3.7a is that despite changing multiple parameters, the obtained field values are still consistent.

3.2 Electric field calculations for the MicroMegas detector

Simulation were done for micromegas with a calendared mesh and a bulk micromegas with a mesh where wires go through each other. The specifications of the same are as follows:

Detector	Mesh wire diameter (μm)	Gap between mesh wires (μm)	Amplification gap (μm)	Drift gap (cm)
MicroMegas	80	120	300	1.2
	28	36	300	1.2
	40	62	300	1.2
Bulk MicroMegas	18	45	192	1.3

Table 3.1

We will refer to each configuration as MicroMegas/ bulk MicroMegas using the notation (mesh wire diameter, gap between mesh wires). For example the first row will be referred to as the (80,120) configuration.

3.2.1 The MicroMegas detector (with a calendared mesh)

The structure of the detector is a standard one, except that the mesh has calendared-like weaves. In neBEM (and COMSOL), this was implemented through 3 designs. The images of the unit cells these designs of the meshes are as follows:

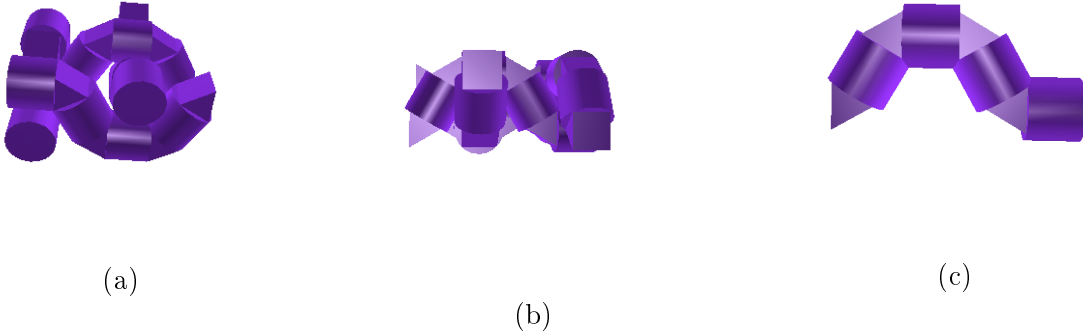


Figure 3.8: (a), (b) Unit cells of the meshes made. (c) A single wire of the unit cell of the mesh. These images correspond to Design 1.

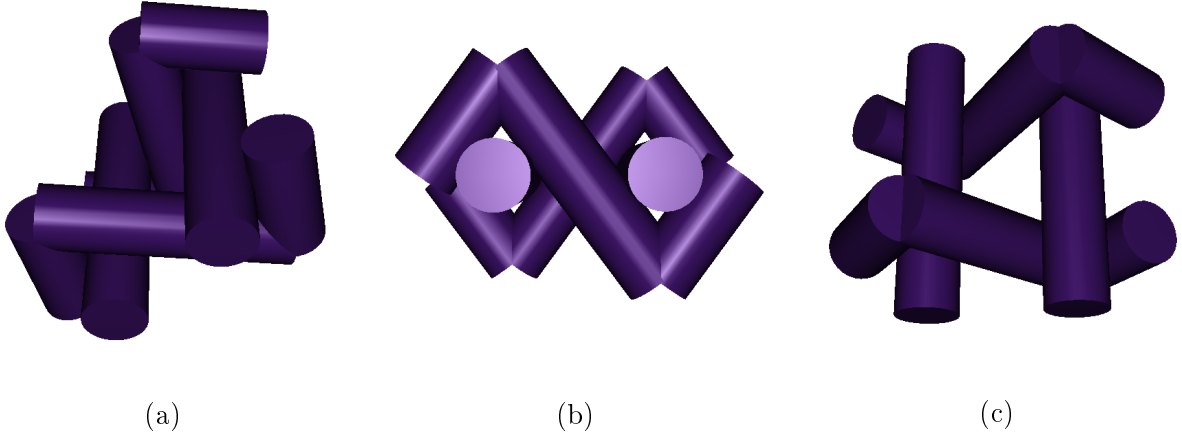


Figure 3.9: Unit cells of the meshes made. These images correspond to Design 2.

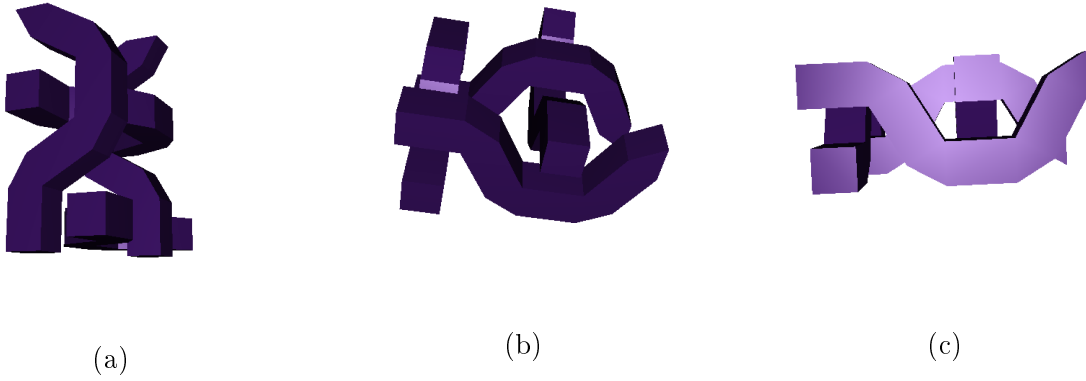


Figure 3.10: Unit cells of the meshes made. These images correspond to Design 3.

The electric field plots were look at, only for Design 1, and reasons for this will be explained later.

For Design 1, the plots for the 3 mesh configurations (refer Table 3.1) are as shown in the following figures:

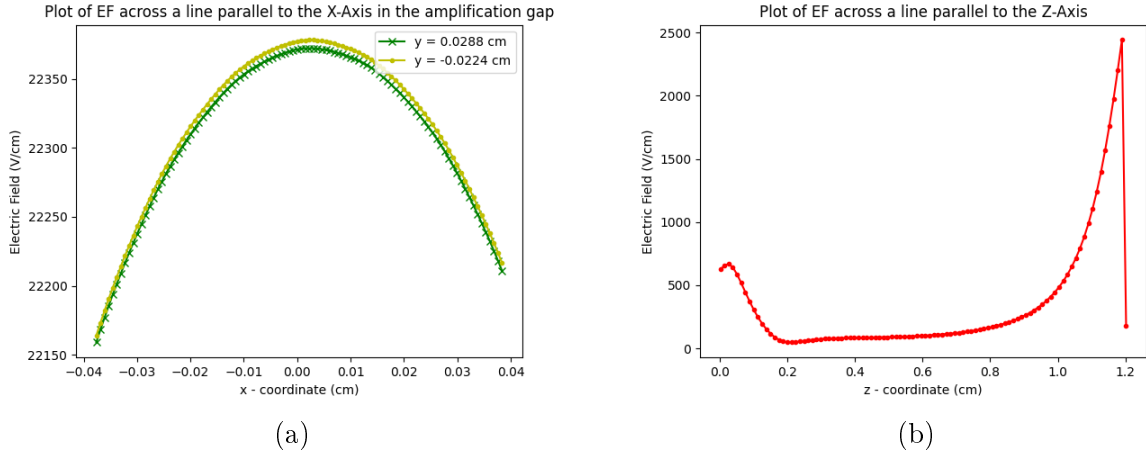


Figure 3.11: The above plots are for Design 1, (28, 36) configuration. Plots for the electric field (a) across a line parallel to the X-axis but at different Y-coordinates and (b) across a line along the Z-axis.

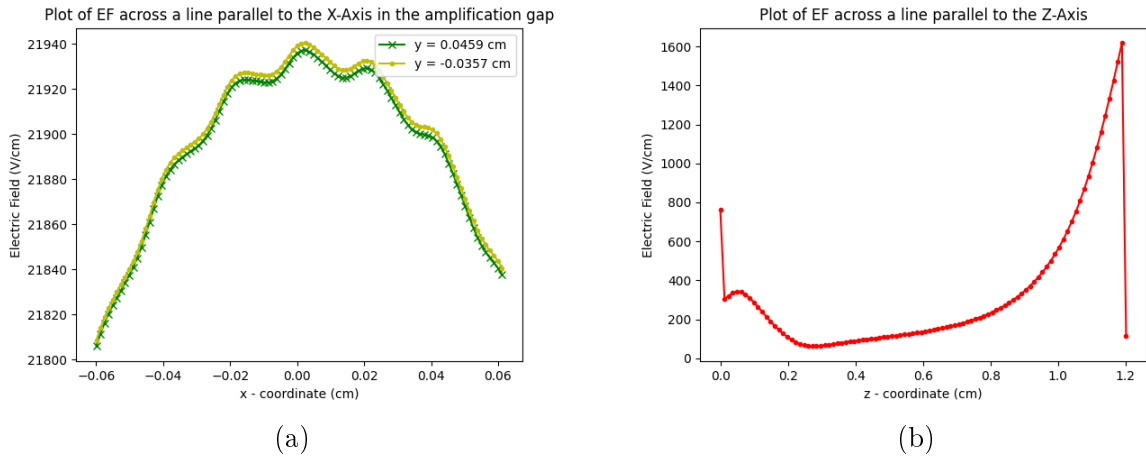


Figure 3.12: The above plots are for Design 1, (40, 62) configuration. Plots for the electric field (a) across a line parallel to the X-axis but at different Y-coordinates and (b) across a line along the Z-axis.

From the above plots, we can see that the (28, 36) configuration seems to display stably-changing electric fields. Further plots made to study this configuration are as shown below:

From Figure 3.15a we can see that as we go towards the mesh, the fields start to fluctuate a bit. And from Figure 3.15b it is evident that for different periodic copies of the unit cell, there are edge effects involved. As explained in Section 3.1.2, we can use such plots to determine the number of periodic copies we need to use to remove edge effects, while still saving on some computation time.

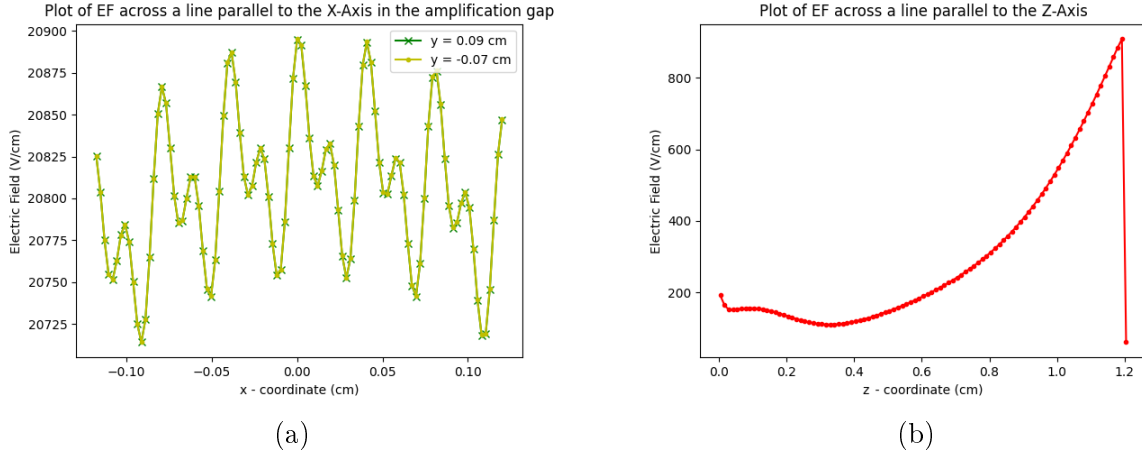


Figure 3.13: The above plots are for Design 1, (80, 120) configuration. Plots for the electric field (a) across a line parallel to the X-axis but at different Y-coordinates and (b) across a line along the Z-axis.

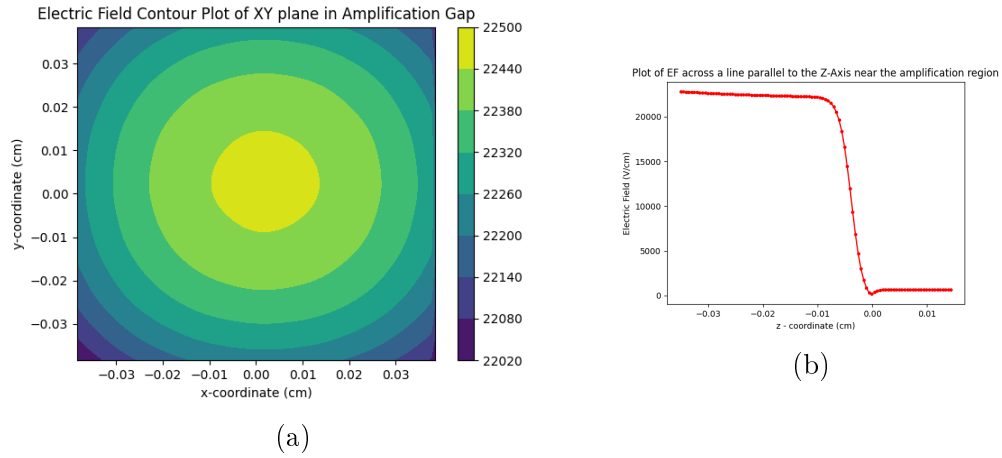


Figure 3.14: The above plots are for Design 1, (28, 36) configuration. (a) The electric field contour plot of the XY plane at a Z-coordinate in the amplification region. (b) Plots of the electric field across a line along the Z-axis but only in the amplification region.

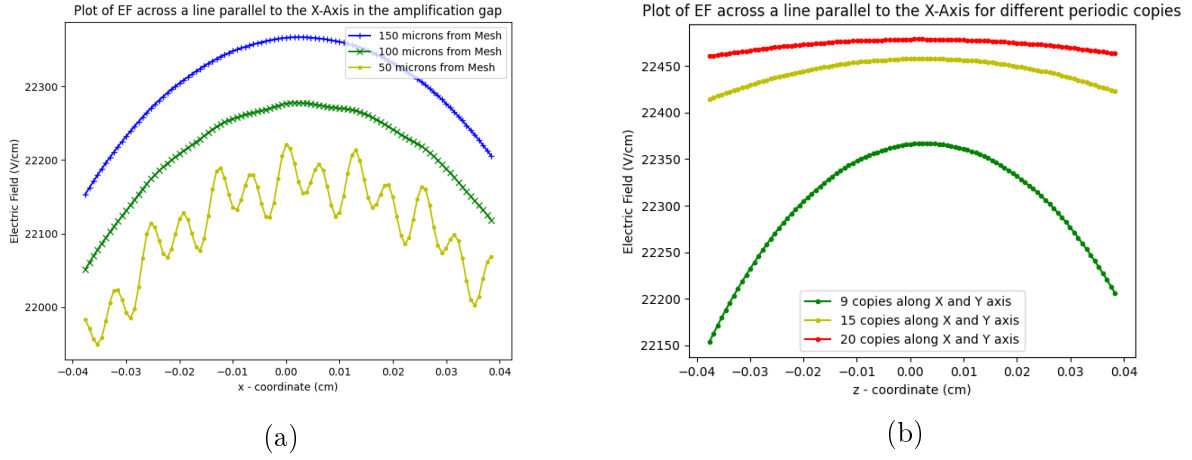


Figure 3.15: The above plots are for Design 1, (28, 36) configuration. Plots for the electric field across a line parallel to the X-axis (a) for different heights (Z-axis) and (b) for different number periodic copies of the unit cell

After subsequent discussion, the group came to a conclusion that the (28, 36), with an opening area of 31.25% is the best mesh to procure. To that effect we went forward to perform gain and signal calculations.

3.2.2 The Bulk MicroMegas detector

The schematic diagram of the mesh unit cell of the bulk MicroMegas is as follows:

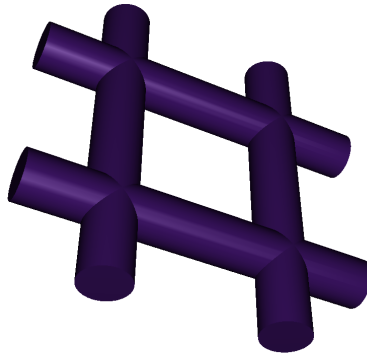


Figure 3.16: A diagram of the mesh's unit cell of the bulk MicroMegas detector.

We simulated the (18, 45) bulk MicroMegas to obtain the following plots:

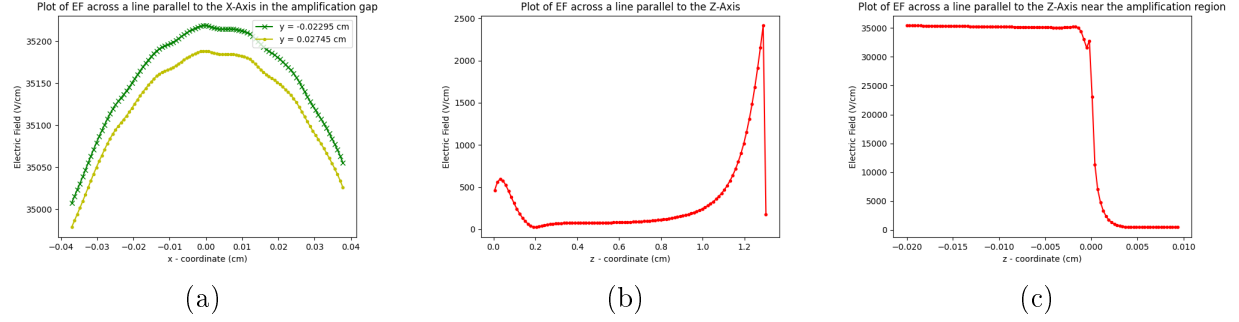


Figure 3.17: Plots of the electric field values for the (18,45) bulk micromegas (a) across lines along the X-axis for different Y-coordinates, across a line along the (b) Z-axis and (c) Z-axis but only in the amplification region.

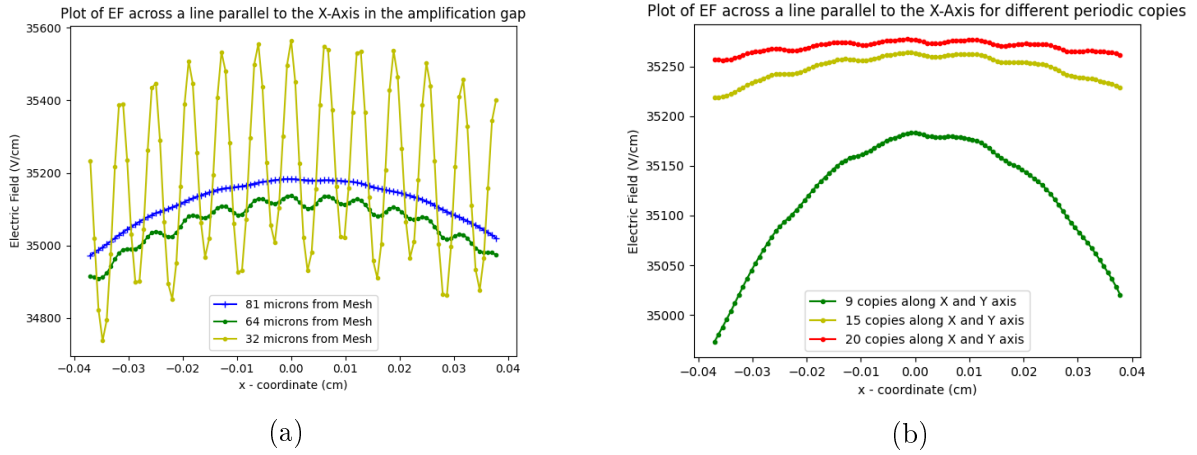


Figure 3.18: Plots for the electric field across a line parallel to the X-axis (a) for different heights (Z-axis) and (b) for different number periodic copies of the unit cell

From Figure 3.18a we can see that as we go towards the mesh, the fields start to fluctuate a bit. And from Figure 3.18b it is evident that for different periodic copies of the unit cell, there are edge effects involved. Similar to what was discussed for the (28, 36) configuration of the MicroMegas detector, we can use such plots to determine the number of periodic copies we need to use to remove edge effects, while still saving on some computation time.

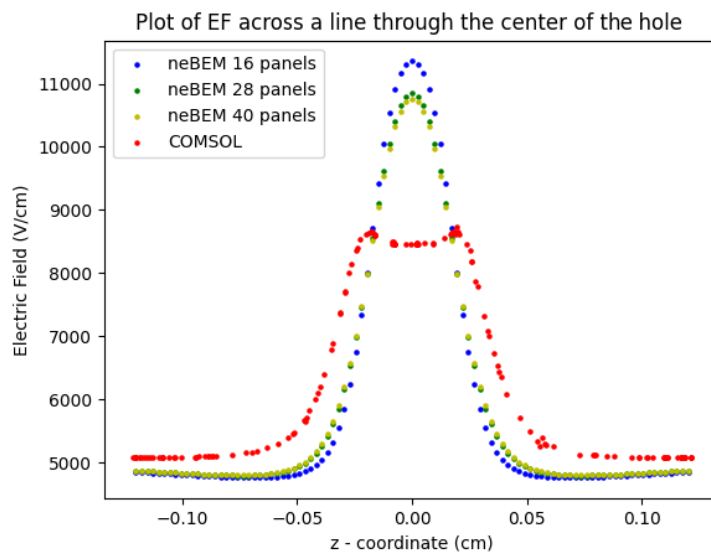


Figure 3.19: Electric field plots for a Thick-GEM for COMSOL and different NEBEM panels.

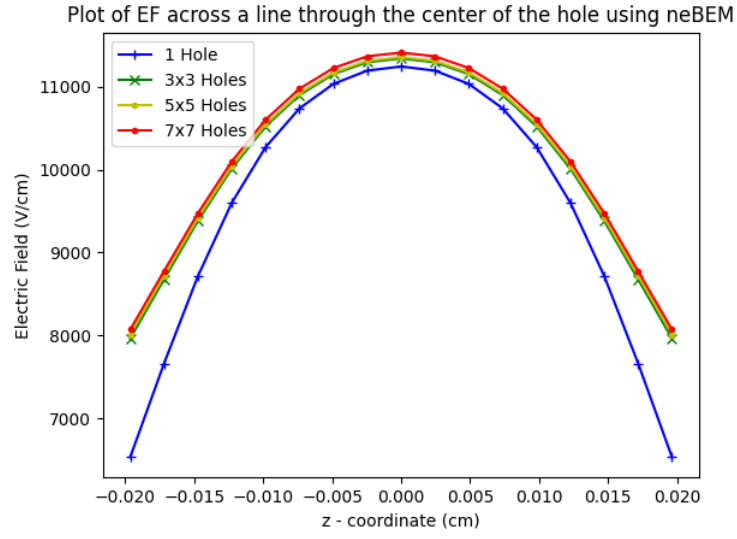


Figure 3.20: Electric field plots using NEBEM for different Thick-GEM sizes.

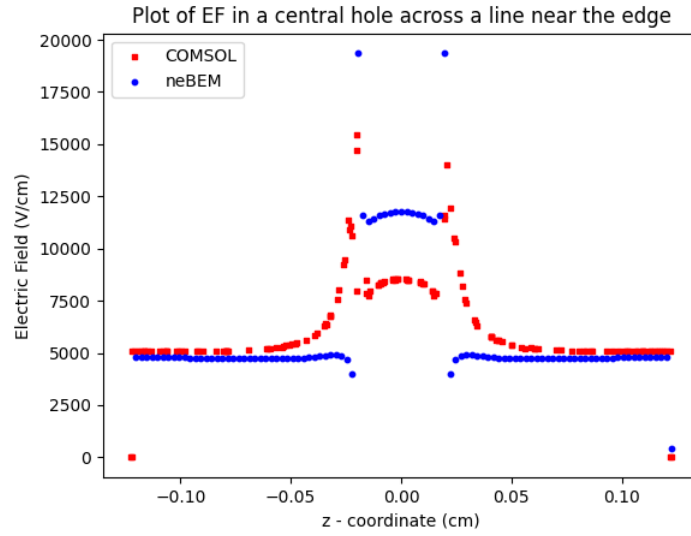


Figure 3.21: Electric field plots near the edge of a Thick-GEM hole using COMSOL and NEBEM.

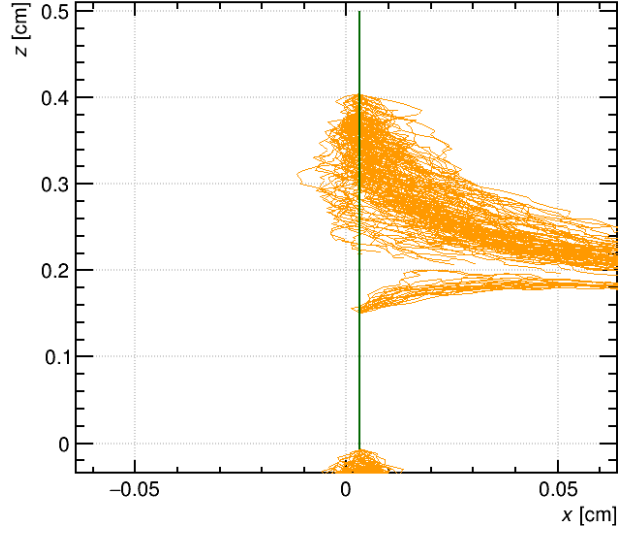


Figure 3.22: Drift lines for an incident electron in the drift region of a Micromegas detector. We expect an avalanche effect and that all electrons reach the anode (go downwards in the above plot), but clearly we do not see expected results.

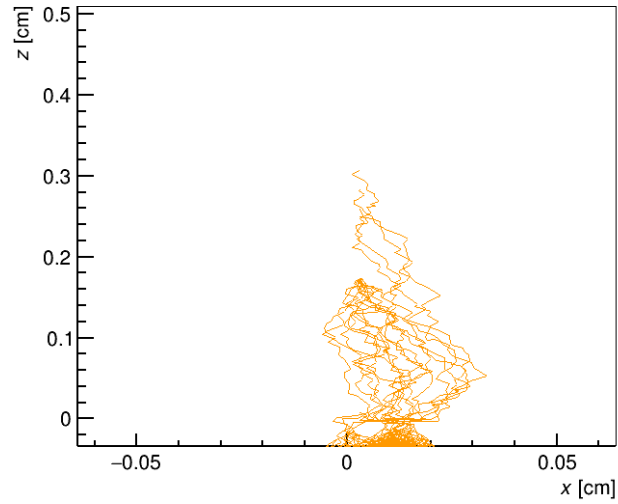


Figure 3.23: Drift lines for an incident electron in the drift region of a Micromegas detector after certain corrections to the code. We see that drift lines match expected results.

We need to note that although we obtained expected results (Figure [3.23](#)), we realised that there is something wrong with Garfield++ NEBEM code and simulations were put at a halt until further corrections were made to the source code.

Chapter 4

Conclusions

During the entirety of the semester, fundamentals of Gaseous radiation detectors and the NEBEM solver was learned. The skills pertaining to simulating Electric field lines and drift lines of a gaseous detector using Garfield++ (NEBEM) and COMSOL was learned. Further studies of the micromegas structure for different mesh structures were left unfinished and this phase of the project can be continued after the required bugs in the source code are corrected. But for the duration of these couple of months during which the project was performed, we successfully created different geometries of Thick-GEM and Micromegas detectors. We created different mesh structures for the Micromegas detector (with a sole focus on calendered meshes) and obtained the electric field contours of the same. We are in process of obtaining drift lines of the same structures and are hoping for changes to be made in the source code at the earliest.

Bibliography

- [1] William R. Leo. *Techniques for nuclear and particle physics experiments: a how-to approach*. Springer, 2nd rev. ed edition, 1994. ISBN: 9783540572800,3540572805,0387572805. URL: <http://gen.lib.rus.ec/book/index.php?md5=fbd221f7f73ebf68ffd16d7c438c93fb>.
- [2] F. Sauli. *Gaseous Radiation Detectors: Fundamentals and Applications*. Cambridge Monographs on Particle Physics, Nuclear Physics and Cosmology. Cambridge University Press, 2014. ISBN: 9781107043015.
- [3] S Bressler, L Arazi, L Molari, M Pitt, A Rubin, and A Breskin. Recent advances with thgem detectors. *Journal of Instrumentation*, 8(12):C12012–C12012, December 2013. ISSN: 1748-0221. DOI: [10.1088/1748-0221/8/12/c12012](https://doi.org/10.1088/1748-0221/8/12/c12012). URL: <http://dx.doi.org/10.1088/1748-0221/8/12/C12012>.
- [4] N. Majumdar and S. Mukhopadhyay. Simulation of three-dimensional electrostatic field configuration in wire chambers: a novel approach. *Nuclear Instruments and Methods in Physics Research Section A: Accelerators, Spectrometers, Detectors and Associated Equipment*, 566(2):489–494, 2006. ISSN: 0168-9002. DOI: <https://doi.org/10.1016/j.nima.2006.06.035>. URL: <https://www.sciencedirect.com/science/article/pii/S0168900206011703>.
- [5] Supratik Mukhopadhyay and Nayana Majumdar. A study of three-dimensional edge and corner problems using the nebem solver. *Engineering Analysis with Boundary Elements*, 33(2):105–119, 2009. ISSN: 0955-7997. DOI: <https://doi.org/10.1016/j.enganabound.2008.06.003>. URL: <https://www.sciencedirect.com/science/article/pii/S0955799708001045>.
- [6] N Majumdar, S Mukhopadhyay, and S Bhattacharya. 3d field simulation in GEM-type structures. *Journal of Instrumentation*, 4(10):P10013–P10013, October 2009. DOI: [10.1088/1748-0221/4/10/p10013](https://doi.org/10.1088/1748-0221/4/10/p10013). URL: <https://doi.org/10.1088/1748-0221/4/10/p10013>.